Growth of shocked gaseous interfaces in a conical geometry

Sanjay Kumar, H. G. Hornung,[a] and B. Sturtevant
Graduate Aeronautical Laboratories 105-50, California Institute of Technology, Pasadena, California 91125

(Received 30 January 2003; accepted 18 July 2003; published 5 September 2003)

The results of experiments on Richtmyer–Meshkov instability growth of multimode initial perturbations on an air–sulfur hexafluoride (SF_6) interface in a conical geometry are presented. The experiments are done in a relatively larger shock tube. A nominally planar interface is formed by sandwiching a polymeric membrane between wire-mesh frames. A single incident shock wave ruptures the membrane resulting in multimode perturbations. The instability develops from the action of baroclinically deposited vorticity at the interface. The visual thickness δ of the interface is measured from schlieren photographs obtained in each run. Data are presented for δ at times when the interface has become turbulent. The data are compared with the experiments of Vetter [Shock Waves **4**, 247 (1995)] which were done in a straight test section geometry, to illustrate the effects of area convergence. It is found from schlieren images that the interface thickness grows about 40% to 50% more rapidly than in Vetter's experiments. Laser induced scattering is used to capture the air–helium interface at late times. Image processing of pictures is also used to determine the interface thickness in cases where it was not clear from the pictures and to obtain the dominant eddy–blob sizes in the mixing zone. Some computational studies are also presented to show the global geometry changes of the interface when it implodes into a conical geometry in both light–heavy and heavy–light cases. © *2003 American Institute of Physics.* [DOI: 10.1063/1.1608011]

I. INTRODUCTION

When two fluids of different densities are in contact with each other and their interface is accelerated impulsively (say by a shock wave) the interface goes unstable and the resulting instability is referred to as Richtmyer–Meshkov (RM) instability.[1,2] It differs from the more familiar Rayleigh–Taylor (RT) instability in the sense that the initial perturbations on the interface grow linearly in time in the beginning. Also, the RM instability does not depend on the direction of acceleration in contrast to the RT instability. The basic mechanism for the growth of initial small scale perturbations in both RT and RM instabilities is the baroclinic generation of vorticity at the interface where pressure and density gradients are not aligned, i.e., $\nabla\rho\times\nabla p\neq 0$. This misalignment deposits vorticity of varying strength on the interface which is responsible for the initial growth of the amplitude of perturbations on it.

As the interface starts to distort, nonlinearities come into play and secondary instabilities like Kelvin–Helmholtz instability develop, which help in generating a wide range of scales of fluid motion. This leads to a turbulent mixing zone at the interface that keeps growing. In RT instability the energy is constantly being supplied by the constant acceleration, while in RM instability the energy for turbulent motions is only supplied at the time of impulsive accelerations, for example, by a shock wave. An example of the occurrence of RM instability is in experiments that aim to achieve inertial confinement fusion (ICF) of deuterium tritium targets.[3–6] ICF is an approach to nuclear fusion that relies on the inertia of the fuel mass to provide confinement. The emergence in the 1970s of inertial confinement fusion as a potential power source has been a major impetus for the study of accelerated and shock-processed interfaces. In such experiments the target is a small hollow spherical pellet which is bombarded with very powerful lasers from all directions. Due to the rapid ablation of the outer surface of the target it behaves like an ablation-driven rocket with an imploding shock propagating inward and setting up RT instability on the interfaces it passes through. RM instability also finds applications in natural phenomena like supernova collapse,[7] pressure wave interaction with flame fronts,[8] and supersonic and hypersonic combustion.[9,10]

Most of the experiments[11,12] so far reported in this area have concentrated on the instability of initially single scale perturbations or multimode perturbations in straight test sections with no area convergence. However, the spherically convergent geometry in the important case of ICF is likely to affect the process significantly. In the ICF experiments or, as a matter of fact, in any other application, it is impossible to generate a perfectly spherically imploding shock. In the case of ICF the sphericity of the shock is destroyed by the imperfections on the capsule due to manufacturing limitations and by the nonspherical symmetry in the laser drive system. The resulting imploding shock may be approximated by piecewise planar imploding shocks. This idea is illustrated schematically in Fig. 1. In three dimensions, piecewise plane shocks of this nature would form a polyhedron, and the shock propagation would bring about complex changes of

[a]Author to whom correspondence should be addressed. Mail Stop 205-45, Caltech, Pasadena, CA 91125. Electronic mail: hans@galcit.caltech.edu

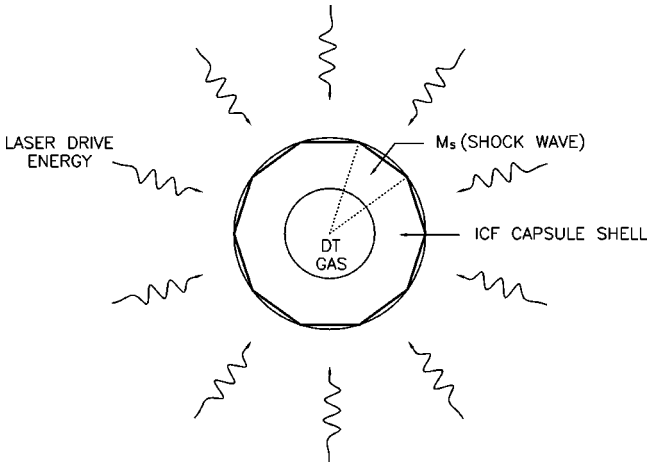

FIG. 1. Schematic of the piecewise planar shock imploding in a sphere.

shape of the shock front, forming different polyhedra and reflected shocks. For the purposes of experimental simulation, the simplest approximation to this situation is to force one such plane shock wave to propagate into a conically convergent geometry. The purpose of the investigation described here is to explore the effect of conical convergence on RM instability with a plane shock and a plane interface. The next paragraph very briefly summarizes previous work in this area.

The small scale random perturbations which are present on the initial interface grow rapidly into the nonlinear regime forming a turbulent mixing zone (TMZ) between the two fluids. Mikaelian[13] adapted the results of constant acceleration experiments of Read[14] to impulsive acceleration and obtained the nonlinear growth of an initially nominally flat interface to be

$$\delta = 0.28A'[u]t, \tag{1}$$

where $[u]$ is the velocity to which the interface is accelerated by the incident shock wave, A' is the post shock Atwood ratio and δ is the interface thickness. Alon *et al.*[15] studied the late-time growth of multimode initial perturbations on the interface. They found that for $A \neq 1$ bubble and spike growth exhibit different power laws. The bubble growth scales with exponent 0.4 for all A while the exponent for spike growth varies with Atwood number. There have been several models describing the RM growth of multimode planar fronts. Dimonte[16] discusses some existing models and reveals their strength and weaknesses. No reliable description of the mixing process in planar geometry has been proposed so far. Existing models are subjects of controversy. Mikaelian's[13] model which assumes homogeneous and isotropic turbulence is attractive solely due to its simplicity. Schneider *et al.*[17] show that RM instability is neither homogeneous nor isotropic. Vetter[11] conducted experiments in a relatively larger shock tube (GALCIT 17 in. diameter horizontal shock tube) on air/SF_6 interfaces with multimode perturbations and obtained linear growth rates after reshock that are in good agreement with Eq. (1). There have been many recent attempts both computationally and theoretically to model the late time growth of RM instability. A very comprehensive review of these studies is presented in a recent review article by Brouillette.[18] The present experiments aim to study the effect of area convergence by measuring the interface growth of multimode initial perturbations in a conical test section. The dynamics of RM instability in converging geometry differs significantly from that in the planar case.[19] The present experimental conditions are the same as those of Vetter[11] including the facility. The results are then compared with results of the nonconvergent experiments of Vetter.

II. EXPERIMENT

The experiments for this study on RM instability are performed in the 434.98 mm (GALCIT 17 in.) diameter horizontal shock tube.[20] The shock tube used in the present experiments is relatively larger than those used by some of the earlier investigators.[2,21–23] This larger size helps minimize effects due to boundary layers on the main fluid dynamical phenomenon under investigation. An existing conically convergent test section (half angle 10°) was attached to the end of the shock tube. The conical test section is made of aluminum with a wall thickness of around 6.86 mm. The larger diameter end of the cone matches the diameter of the shock tube and the cone is truncated at a diameter of 90.42 mm. In order to further narrow down the smaller diameter end, an end piece was made taking the diameter down to 19.05 mm. The length of the conical test section with the end piece was 1183.89 mm. For flow visualization it was necessary to fit the cone with windows. The location of the windows along the axis of the conical test section was chosen to capture the interface near the position at which it comes to rest at the conditions of the experiment. The conditions were chosen, for suitable comparison with nonconverging geometry, to coincide with those of Vetter,[11] i.e., incident Mach number ($M_S = 1.55$). This location was determined by preliminary numerical simulations.

For the initial experiments, three pairs of opposing circular windows were mounted on the surface of the cone as shown in Fig. 2. In preliminary attempts to capture the interface in the three window locations by schlieren visualization, it turned out that the turbulent mixing zone at the interface grows to more than the window size in the second and third locations (first location refers to the one that is closest to the initial interface location). In order to overcome this difficulty, two pairs of rectangular windows were fitted at the second and third locations. The clear aperture of these windows was a 203.2×55.88 mm rectangle. The shape of the cross-section at the center of the window in the plane perpendicular to the generator passing through the center of the window was the same as that of the circular windows at the same location. The length of the rectangular windows is such that along the axial direction the windows at the third location begin where those at the second end. In the circumferential direction the windows at the third location are rotated by 45° to those at the second. Figure 3 shows the cone with the rectangular window at $x = 533.4$ mm.

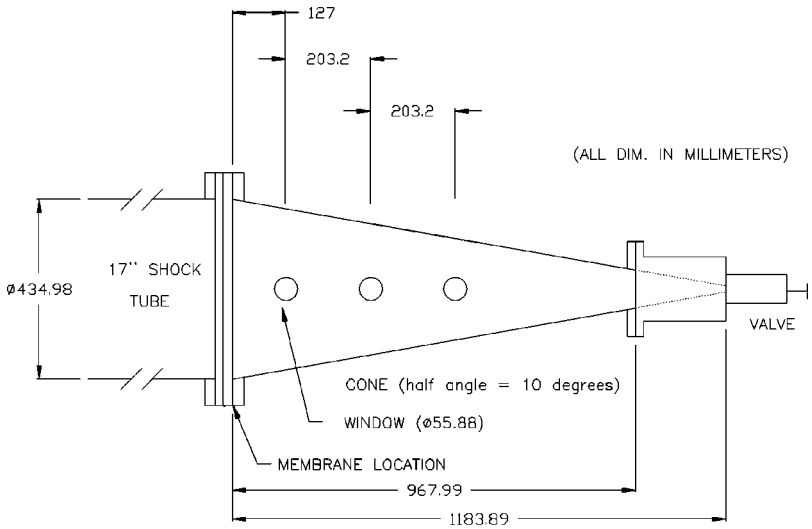

FIG. 2. Schematic of the conical test section with circular windows attached to shock tube.

The initial interface was formed by a thin polymeric membrane sandwiched between two circular wiremesh frames. The average thickness of the membrane in our experiments was 1.5 μm, as in the experiments of Vetter.[11] Recently, Erez *et al.*[24] did experiments at a shock Mach number of 1.25 to study the effect of the thin membrane on the time evolution of the RM instability. The main conclusions of this set of experiments were that the membrane has a significant effect on the initial growth, but when the amplitude becomes large and the TMZ growth becomes fully nonlinear, it has negligible effect and the results agree with numerical simulations. In the present study, the effect of membranes and wires has not been investigated. However, the authors would like to refer to a study by Prasad *et al.*[12] who conducted experiments in the same facility and under same conditions except that single mode configurations were used. The wire spacing in their wiremesh was the same as in the present investigation. They studied the effects of wiremesh and membrane on turbulent mixing and reasoned that the wiremesh and membrane have opposite effects on growth rates with membrane fragments acting to supress the mixing process and wiremesh enhancing it. The authors believe that the same effects prevail in the present investigation too as the experimental conditions as far as the initial interface formation technique is concerned are the same. The circular frame that supports the wire mesh is made from aluminum with internal and external diameters of 434.98 and 458.22 mm, respectively (see Fig. 4). The thickness of the frame is 5.08

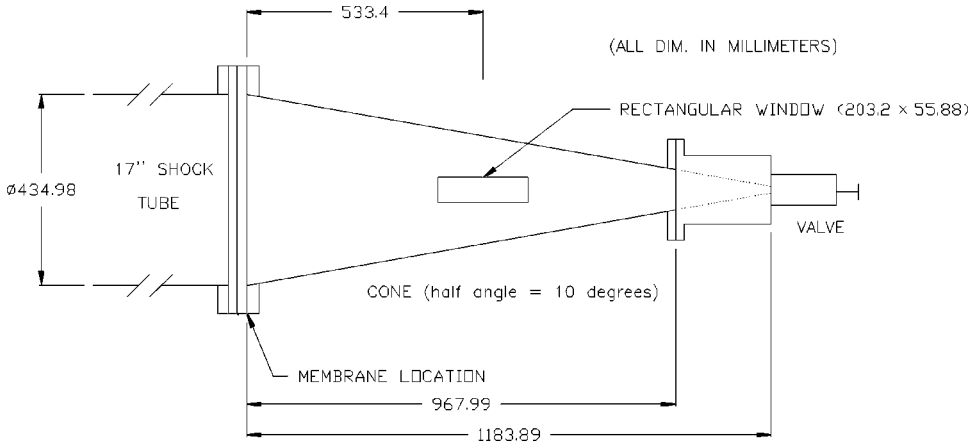

FIG. 3. Schematic of the conical test section with rectangular window attached to shock tube.

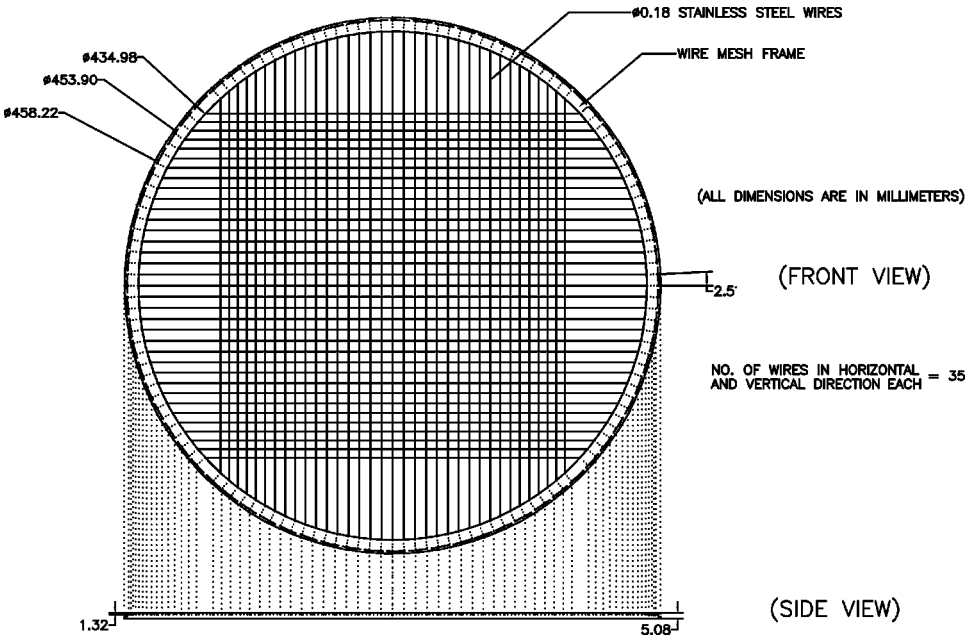

FIG. 4. Wiremesh frame.

mm. On the periphery of the frame along the side a groove 2.16 mm deep is machined. One side of the groove is 1.32 mm from the face of the frame. Along the groove 144 radial holes of 1 mm diameter are drilled to support the wires. Thirty-five stainless steel wires of diameter 0.18 mm attached to the frame span it in mutually perpendicular directions. The wires were necessary to support the flimsy membrane because of the large cross-section of the shock tube. The wires were separated by 1 mm in the axial direction, i.e., on either side of the membrane. The separation between the horizontal and vertical wires was the same as that in the experiments of Vetter.[11] Prior to each run as in Vetter's experiments, the membrane was pushed slightly into the wiremesh, with an estimated amplitude of about 1 mm. For more details of the wiremesh frames and general setup the reader is referred to the thesis by Kumar.[25] The origin of the coordinate system is chosen to be at the center of the initial interface with the x-axis pointing into the cone.

Flow visualization to study the growth of RM instability was done both by schlieren and laser-induced scattering (LIS) from a laser sheet. The schlieren system was used with a spark gap light source. The spark source generates a flash of white light of approximately 0.5 μs duration. Figure 5 shows schematically the schlieren system setup. For the LIS experiment, a Nd–Yag pulsed laser (Model: Tempest-Gemini PIV from New Wave Research, Inc.) was used to produce a very thin (1 mm) laser sheet. Olive oil mist (droplet size approximately 1 μm) produced from a fog generator designed by DLR, Germany, was used for this purpose. Since the mist can only be produced by passing high pressure gas in the fog generator, it was not possible to directly pass the test gas through it because of the presence of the fragile

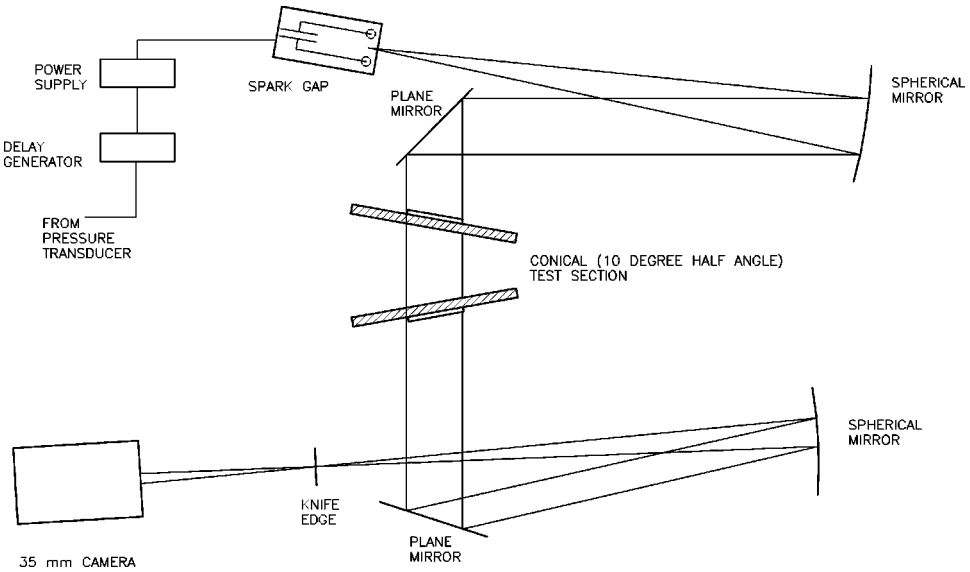

FIG. 5. Schematic of the schlieren setup.

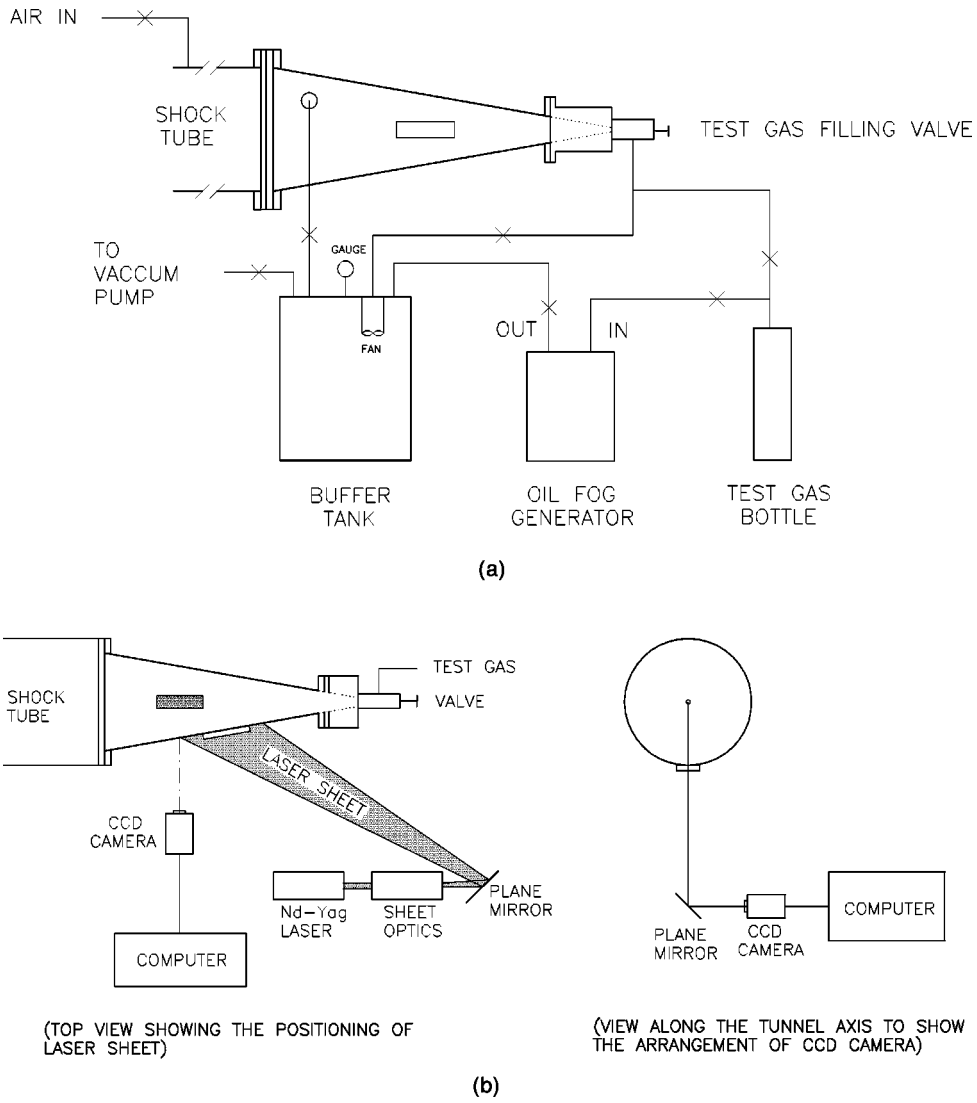

FIG. 6. Schematic of the laser induced scattering setup. (a) Seeding technique. (b) Laser sheet and camera locations.

membrane. A new seeding technique was designed in which a buffer tank was first filled with the test gas and mist. The pressure in the tank was then brought to the test section gas pressure of 23 kPa. The circuit connecting the test section and the buffer tank was then opened and a fan helped mix the test gas in the test section and the buffer tank. Figures 6(a) and 6(b) show the schematic of seeding and flow visualization technique. The run procedure and the instrumentation were similar to those of Vetter[11] except that there were no pressure transducers in the conical test section. The pressure transducers upstream of the interface were used to trigger the data acquisition, spark gap light source and laser. Helium was used as the driver gas in the shock tube. For the present run conditions the expansion wave from the driver section overtook the incident shock in the test section, so behind the shock the pressure decreased at a measured rate of 1.5 kPa/ms. Thus the impulsive acceleration by the shock was followed by a small constant deceleration, superposing a small stabilizing RT effect on the RM growth. This effect was also present in Vetter's[11] experiments. Since these experiments are in a converging geometry, postshock deceleration is always present.

III. RESULTS

The flow physics of the present problem in a conical geometry as compared to the one in a straight test section is further complicated by the diffraction of the shock wave as it enters the cone. The Mach number and cone angle of the present conditions ensure a Mach reflection at the cone wall. The reflected shock initially interacts strongly with the interface, producing a change in its overall geometry. The dynamics of the interface mixing is further complicated by the subsequent interaction with the rereflected waves from the axis and the wall. The diffraction of the shock wave in the 10° half-angle cone was investigated in detail in the same shock tube by Setchell.[26] A schematic of the shock wave evolution is shown schematically in Fig. 7.

Figures 8(a) and 8(b) show the spark schlieren pictures of the TMZ in the first window location at two different

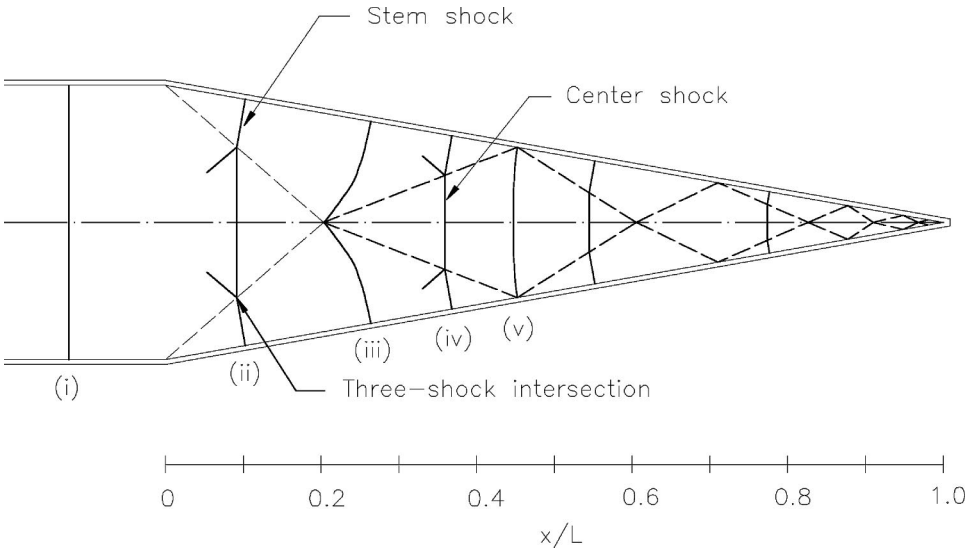

FIG. 7. Diffraction of the incident shock wave: (i) plane initial shock; (ii) Mach reflection on the cone wall; (iii) stem-shock intersection on the cone axis; (iv) Mach reflection on the cone axis; and (v) start of the second diffraction cycle. — — —, trajectory of the three shock intersection. Flow is from left to right [after Setchell (Ref. 26)].

times. The interface appears dark because of the combination of the schlieren effect and the scattering of light from the field of view by membrane fragments. The interface thickness is measured visually from the photograph (as shown in Fig. 8). The interface thickness, defined as the thickness from the front to the back of the interface, is represented here by δ. The x-location of the interface is defined to be the distance from the initial location of the interface to the middle of the TMZ. The time $t=0$ denotes the time when the incident shock wave interacts with the interface. The universal bubble and spike feature of this instability is not very evident here at late times because the bubbles tend to flatten out possibly due to the deceleration[27] and the spikes tend to break up due to the Kelvin–Helmholtz instability along their boundaries. It is also hard to see the 3-D disturbances with schlieren visualization. Figure 9 at window location 2 gives another clue that the interface is spread out near the wall which possibly can corrupt the schlieren flow visualization since the technique uses line of sight integration.

To monitor the growth of the TMZ, it is photographed at the second ($x=330.2$ mm) and the third window ($x=533.4$ mm) locations. Figure 9 shows the TMZ in the second rectangular window location along with the numerically simulated result from computations using the AMRITA[28] system. It should be kept in mind that the numerical calculations are Euler calculations and hence they give no idea of the viscous effects in the mixing process in the TMZ, or of boundary layer effects near the wall. Hence the TMZ thickness cannot be inferred from these simulations. The reflected shock interacts strongly with the interface during the initial stages, depositing vorticity of the appropriate sign. This causes the interface to become curved as is evident in Fig. 9(b). The main central shock, reflected shock and the Mach stem are clearly visible in this figure.

Another measure of interface thickness called the ''geometric thickness'' is defined in numerical simulations. This definition is motivated by the fact that in numerical simulations the interface curves into or away from the apex of the cone depending on the sign of the density difference across the interface. When the interface curves towards the cone apex, it is defined to be the axial distance from the front of

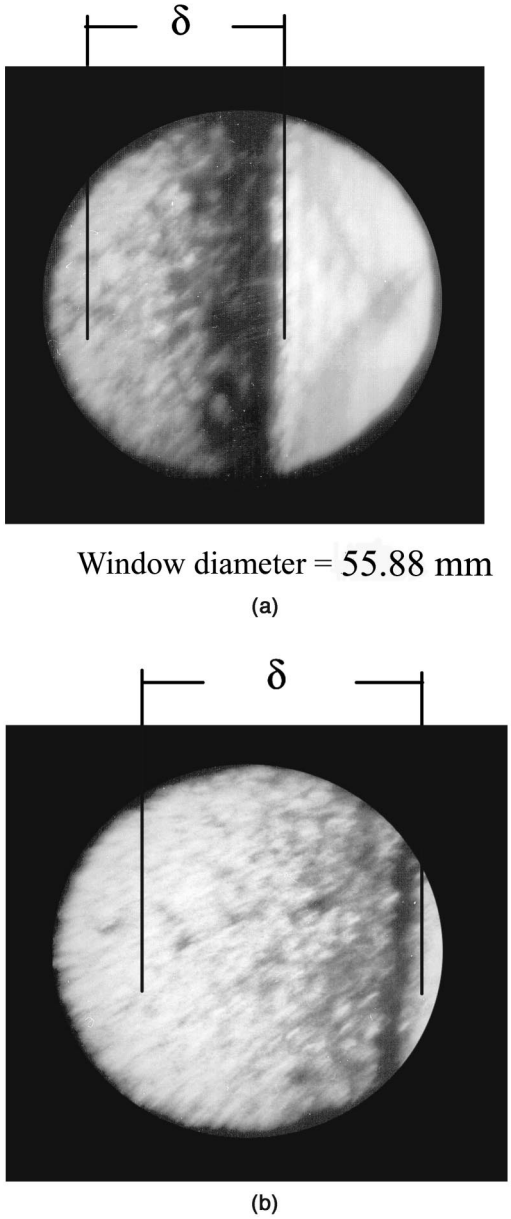

FIG. 8. (a) Schlieren image of TMZ at $x=120$ mm and $t=0.95$ ms. (b) TMZ at $x=135$ mm and $t=1.04$ ms. Flow is from left to right with air–SF_6 (light–heavy) configuration.

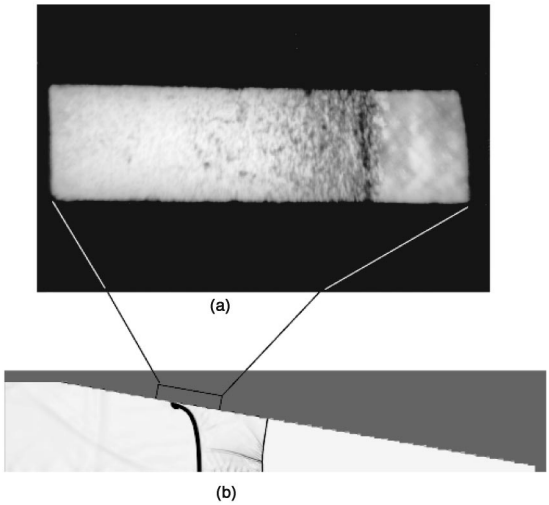

FIG. 9. (a) Schlieren image of TMZ at $x=336$ mm and $t=2.42$ ms from run no. Rshot 67. (b) Numerical simulation result at about same x/L. Flow is from left to right with air/SF_6 (light–heavy) configuration; the window location is also shown on the numerical data.

the interface on the cone centerline to the curved rear boundary near the wall. This ''geometric thickness'' is illustrated for the numerical result of Fig. 9(b) in Fig. 10.

In the previous experiments on RM instability, the interface thickness is measured ''visually'' from photographs[2,11,14,21,29–32] and is called the ''visual thickness.'' In the present experimental conditions with conical geometry, the front of the interface advancing into the test section is very well demarcated but the rear boundary is rather diffuse as may be seen in Fig. 9(a). A technique was therefore devised to analyze the interface using image processing. The visible image in the rectangular window [2164×526 pixels in size for Fig. 9(a)] was digitized and the average gray-scale intensity of each pixel column was computed. These average intensities are plotted against the horizontal distance in pixels (Fig. 11). An intensity of 0 is the darkest and 256 is the brightest. The average intensity shows a sharp gradient at the advancing front of the TMZ as expected. Inside the TMZ, the average intensity fluctuates due to the schlieren effect of the random density variation produced by the mixing blobs. At some distance behind the advancing front, the fluctuations in the intensity die down and the intensity varies smoothly. The rear end of the TMZ can be taken to be the location where these fluctuations in intensity seem to stop (with an uncertainty of 10%–15%). This technique is illustrated in Fig. 11 for the TMZ shown in Fig. 9(a). This technique was applied to the schlieren pictures of the TMZ at the second window location because it was at this location that the TMZ had a long diffuse rear boundary. The ''visual thickness'' obtained

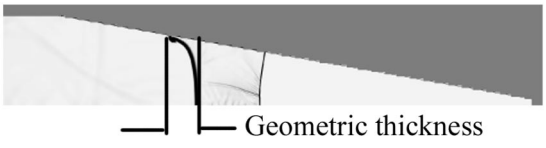

FIG. 10. Geometric thickness defined.

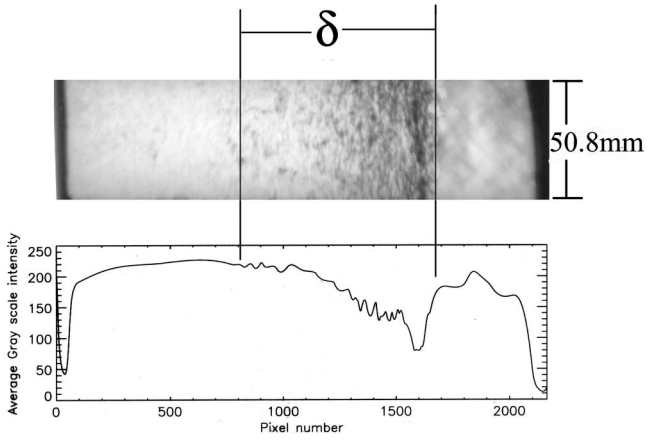

FIG. 11. Illustration of image processing technique to fix the boundaries of TMZ for the TMZ shown in Fig. 9(a). The image size is 2164×526 pixels which corresponds to physical dimension of 208.28×50.8 mm.

by observing the photographs matches closely to the ones obtained by this image processing technique to within 10% to 15%. The ''visual thickness'' and the thickness determined from this technique are tabulated in Table I. The technique obviously works in cases where both the front and rear of the TMZ are clear as in Vetter's[11] pictures.

Figure 12(a) shows the mixing zone at the third window location. It is clear from the figure that the mixing zone completely fills the viewing window. In order to locate the other boundary of the TMZ, the experiment was repeated with the same settings except that the visualization was done in the second rectangular window. The second and third rectangular windows are located side by side along the axial direction, though they are offset in the circumferential direction. The third rectangular window can be viewed as continuation of second rectangular window. Figure 12(b) shows the schlieren image of the TMZ in the second rectangular window corresponding to the settings of Fig. 12(a). It is clear that there is no mixing visible in this image and hence the TMZ thickness can be taken as the mixing zone visible in Fig. 12(a) where the rear of the mixing zone is bounded by the window wall. The two photographs in Fig. 12 were taken in different runs and hence the absence of mixing in Fig. 12(b) does not mean there was absolutely no mixing going on behind the rear boundary of the window in Fig. 12(a). The error in this mixing zone width is equal to the scatter in the front of the TMZ's visible in the repeatability demonstration (Fig. 15). Figure 12(a) also shows clearly the intersection of reflected shocks at the centerline of the cone. The interface moves into the cone and comes to a stop at an axial location

TABLE I. Visual thickness and thickness from image processing.

Run no.	Mach no. ±0.01	Visual thickness (mm)	Thickness from image processing (mm)
Rshot 67	1.56	91	81.2
Rshot 81	1.57	102	93.67
Rshot 82	1.56	107	107
Rshot 95	1.55	93.13	77.6
Rshot 97	1.57	115	100.1

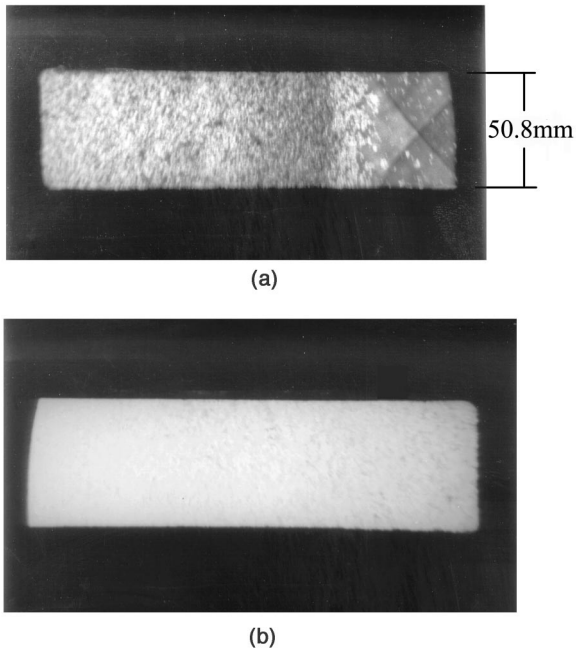

FIG. 12. (a) Schlieren image of TMZ at $x=506$ mm and $t=3.68$ ms, $M_S=1.57$. (b) Schlieren image of TMZ in second rectangular window at the same settings as in (a) (the flow is from left to right).

depending on the Mach number. This is clear from the $x-t$ diagram (see Fig. 13) computed from the numerical computations for incident Mach number of 1.56 in the light–heavy case. Figure 12(a) also shows the TMZ before the central reflected shock interacts with it a second time. Similarly the growth of the TMZ was also observed at a Mach number of 1.39 in the first and third windows. In order to see how the

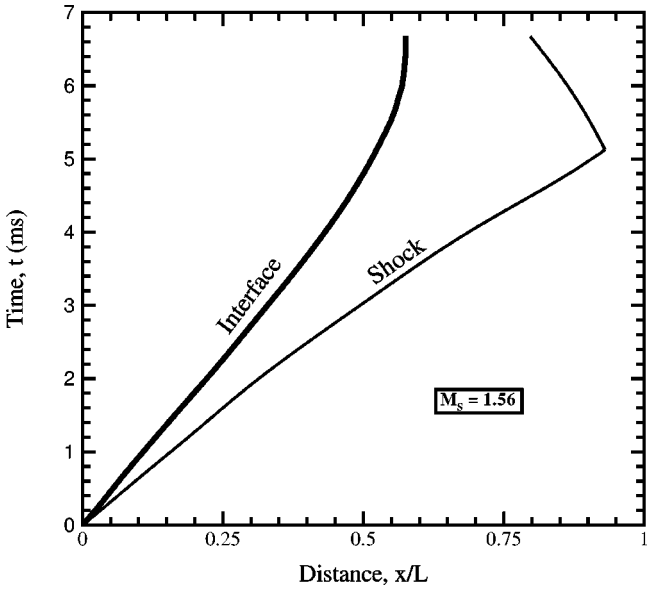

FIG. 13. $x-t$ wave diagram in the conical geometry showing the interface and shock trajectory in light–heavy configuration at Mach number of 1.56. Here L is the length of the cone and x coordinate is measured from the initial interface location into the cone. The $x-t$ diagram was drawn from the numerical simulation performed on AMRITA (Ref. 28). The trajectories refer to the location of interface–shock on the cone axis.

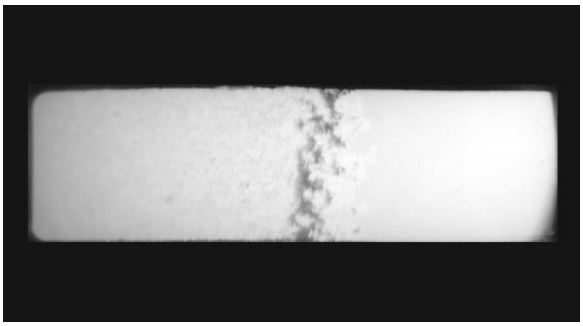

FIG. 14. (a) Schlieren image of air–air interface in the second window location at $x=330.2$ mm and $t=1.52$ ms, $M_S=1.59$, showing the membrane fragments getting clustered in front of the interface. The flow is from left to right.

membrane appears in these schlieren pictures (with the same settings as of air–SF_6 interface pictures), experiments were conducted with air on both sides of the interface. Figure 14 shows the air–air interface. It is clear from the figure that the membrane fragments appear as dark areas near the front of the interface because they get clustered together there. When the same fragments are not clustered they appear as white areas. This clustering of the fragments is also evident in the laser induced scattering image of Fig. 21(b).

The growth of the TMZ obtained in this fashion clearly depends on the repeatability of the experiments as each schlieren picture is obtained from a different experiment. The quality of the repeatability in the present experimental conditions is shown in Fig. 15. The maximum separation between interface advancing fronts in Fig. 15 is about 15 mm, which is due to the variability in the Mach number.

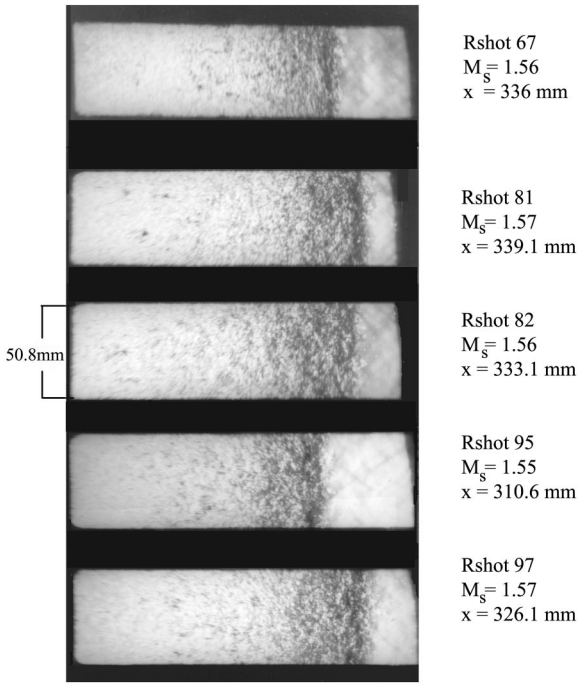

FIG. 15. Demonstration of the extent of repeatability of the experiments in second rectangular window location.

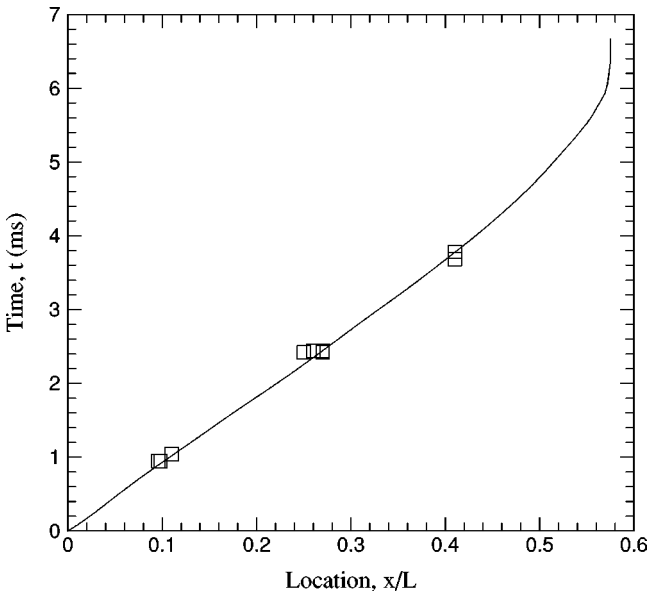

FIG. 16. $x-t$ diagram from numerical computations along with the experimental data points at Mach number of 1.55. Solid line, Amrita computations at $M_S=1.56$; □, experimental data at $M_S=1.56$.

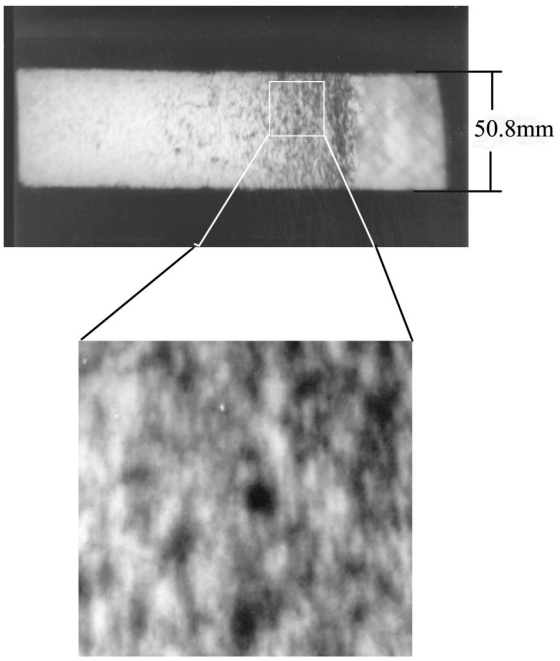

FIG. 17. A 256×256 pixel image sampled from the TMZ of Fig. 9(a) for dominant scale size determination by image processing.

Having obtained the interface location, thickness and timing at three locations, the $x-t$ diagram was plotted featuring the experimental data points for Mach number 1.55 and the numerical computations. Figure 16 shows such a plot. It is clear that all the data obtained experimentally are from the region to the left of where the interface is rapidly decelerated to zero velocity. During the period of experimental observations the interface moves at a very nearly uniform velocity. This eliminates the possibility that the strong RT effect that may be expected to accompany the subsequent rapid deceleration influences the data.

A. Dominant scale size determination

The schlieren pictures show dark blobs which are created by the refraction of light through density gradients in the TMZ and appear as scattered dark spots on the pictures involving air–SF_6 interface. The size of these blobs gives an estimate of the dominant scale of eddies which are involved in the mixing process. It should be kept in mind that the schlieren effect results from the density gradients due to mixing of the gases and also to a smaller extent from membrane fragments. To get an idea of this blob size, a 256 ×256 pixel size image was sampled from the upper-right corner of the mixing zone shown in Fig. 9. It is also shown in Fig. 17. The surface plot of its Fourier power spectrum density (psd) and its radial power density is shown in Fig. 19. The wave number is normalized in such a way that the wave number in the plots represents the number of wavelengths in the 256 pixel size domain. To obtain the radial power spectral density plot from the surface plot of psd, the average power in rings of two wave number unit width was assigned to the radius at the middle of the ring. This procedure is illustrated schematically in Fig. 18. The maximum power density occurs at a wave number of 3 [see Fig. 19(b)] implying that there are three waves of dominant wavelength in 256 pixels which translates to a dominant blob size of around 4 mm in actual scale. This size is about half the spacing (8 mm) between the wires of the wire-mesh frame which holds the polymeric membrane forming the initial interface separating the two gases. The same process was repeated by taking portions of image from various places of the same TMZ image and also at the various axial locations of the observation windows. The dominant size of these structures did not vary, i.e., it was 4 mm as found earlier. Figure 20 shows the image of Fig. 17(a) with markers indicating the dominant scale–eddy–blob size of 4 mm thus obtained from the radial power spectral density plot.

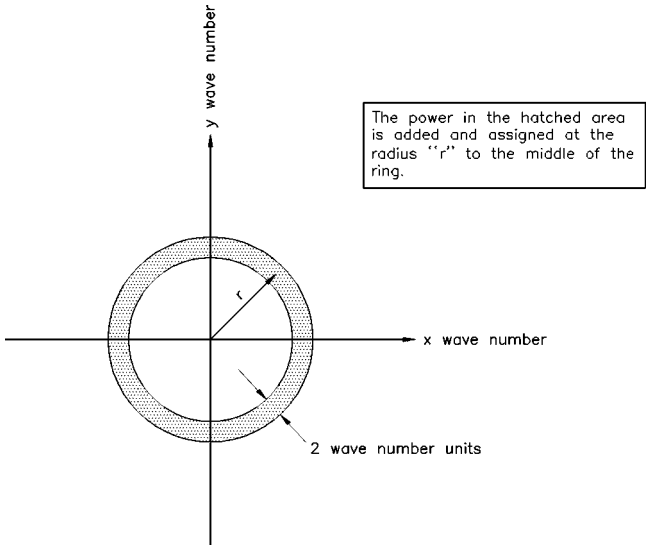

FIG. 18. Schematic of the procedure to obtain radial power spectral density from surface psd plot.

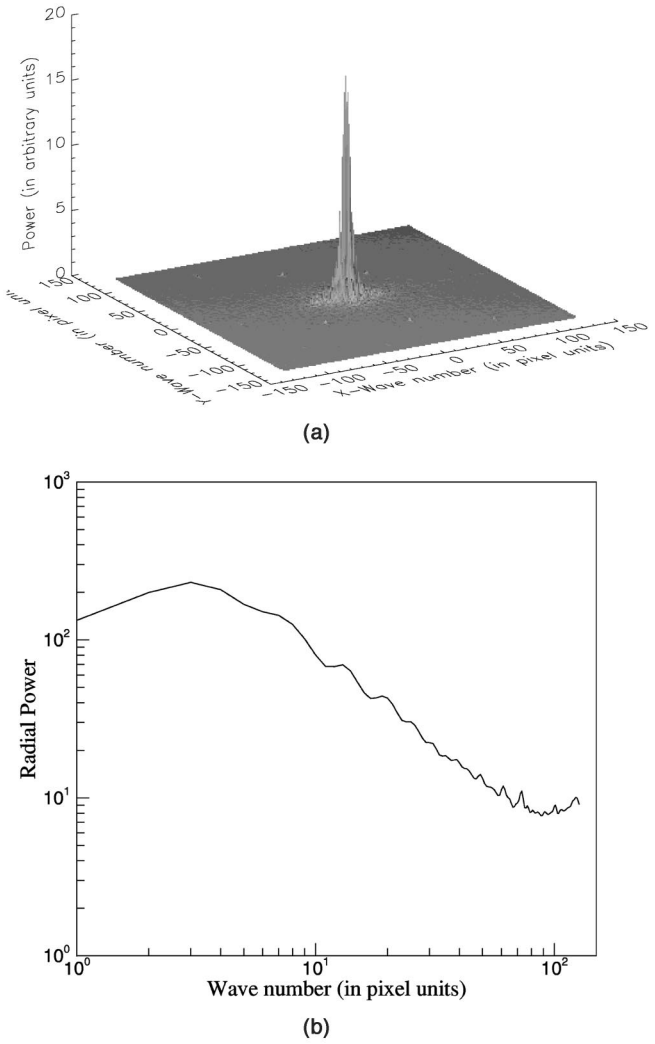

FIG. 19. (a) Surface plot of power spectral density for sampled image of Fig. 17. (b) Radial power spectral density.

B. Laser-induced scattering result

As is evident from the numerical simulation result in Fig. 9(b), the interface bends near the walls. Since the schlieren pictures give the line of sight integrated effect, it is possible that the TMZ thickness measurements are affected by this curvature. The only way to eliminate this effect is to study the TMZ with sheet optics techniques. To probe the TMZ in detail, laser-induced scattering experiments were attempted (see Sec. II for details of the setup and the difficulties encountered in doing this experiment). In this experiment, the test gases were helium and air in the heavy–light configuration. Since the absolute values (0.67 and 0.76) of Atwood numbers of air–SF_6 and air–He are similar, the mixing zone width is expected to be similar at least before the arrival of the main central reflected shock and onset of rapid deceleration. The global curving of the interface does depend on the sign of the Atwood number. The helium in the test section is seeded with olive oil fog particles. Figure 21(a) shows the image of the light sheet in the test section seeded with oil particles and helium, and Fig. 21(b) shows the TMZ as it appears in front of the observation window. The membrane fragments clearly scatter lots of light and hence are a source of noise. But the fine bright particles at the rear of the TMZ represent the oil droplets. This at least gives an idea of the extent of mixing in TMZ (visual thickness is 87.3 mm in that picture) in that condition. The curving of the interface near the wall is not visible because the viewing area is too small. The extent of the mixing zone in this image which shows the full rectangular window of size 203.2 $\times$55.88 mm is similar to the one in Fig. 9(a) where the vi-

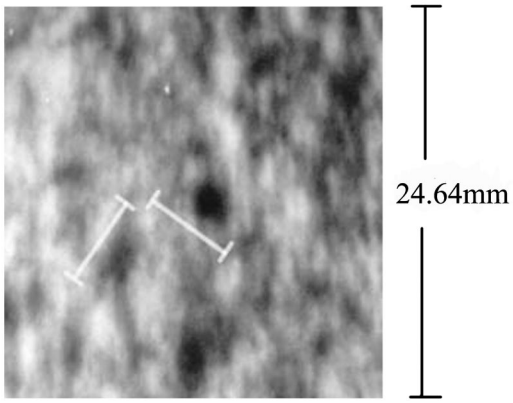

FIG. 20. Picture of the sampled image in Fig. 17 with markers indicating the dominant size of scales obtained from the maxima in radial power spectral density plot of Fig. 19(b).

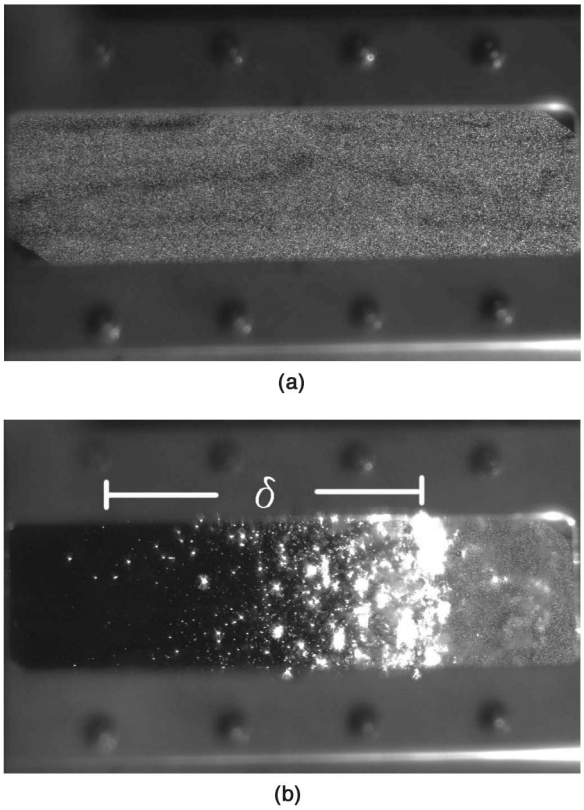

FIG. 21. Laser-induced scattering experiment (heavy–light configuration) in second window location at $x=330.2$ mm. (a) Laser sheet in the test section with helium and olive oil fog particles. (b) The TMZ with membrane fragments visible as relatively big bright scattering spots and very fine bright dots representing the seeded oil particles from the right, $t=1.25$ ms, $M_S=1.60$.

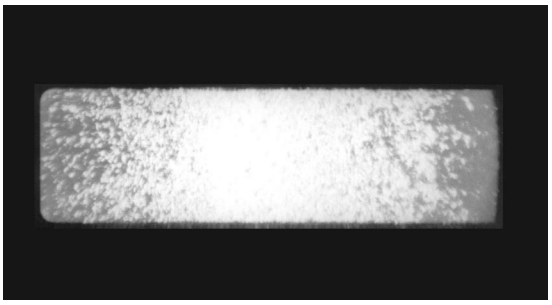

FIG. 22. Schlieren image of air–helium interface in second window location at $x=330.2$ mm, $t=1.25$ ms, $M_S=1.60$ (flow is from left to right).

sual thickness is 91 mm. The mixing zone in Fig. 21(b) shows that in the center of the test section the TMZ does not have a well demarcated rear boundary but is rather diffuse. The schlieren picture of the TMZ corresponding to the laser induced scattering image of Fig. 21(b) is shown in Fig. 22. The flow visualization picture in Fig. 21(b) also shows that visualizing the TMZ by the light scattering technique suffers from the noise generated by the membrane fragments. A more effective way of solving this problem would be to use laser-induced fluorescence by mixing a fluorescent oil soluble dye (for example, pyrromethene-597 or rhodamine-640 are easily excited by 532 nm Nd–Yag laser in oil) with olive oil in the fog generator and using an appropriate filter in front of the CCD camera in order to eliminate the light scattered from the membrane fragments at the laser wavelength. This was attempted with the result that fluorescence was too weak to be detected by ordinary CCD camera, requiring the use of intensified CCD camera. As a result, further experiments with sheet optics were abandoned.

C. Effect of transverse reflected waves on the growth of small initial perturbations: An inviscid computational study

As the shock enters the cone, it is reflected from the cone corner in a Mach reflection so that a triple point is created on the shock wave. As a result, the reflected shock wave originating at the triple point propagates transversely across the cone, focusing onto and reflecting from the cone axis. In doing so, these transverse waves interact with the interface behind them. This interaction gradually becomes weaker as the triple point moves farther from the interface. It is the baroclinic deposition of vorticity from these interactions at the early times which lead to the global curving of the interface [as is clearly evident in the Fig. 9(b), where the interface curves towards the apex of the cone].

In order to examine the effect of these transverse waves on small initial sinusoidal perturbations, an axisymmetric computational study was undertaken at Mach number of 1.56 in light–heavy configuration using AMRITA[28] (see Sec. IV for a brief description) in both conical and straight cylindrical geometry. The growth of the perturbations in these calculations results solely from the vorticity deposited by the initial interaction of the incident shock with the perturbed interface. The calculations are inviscid and hence do not

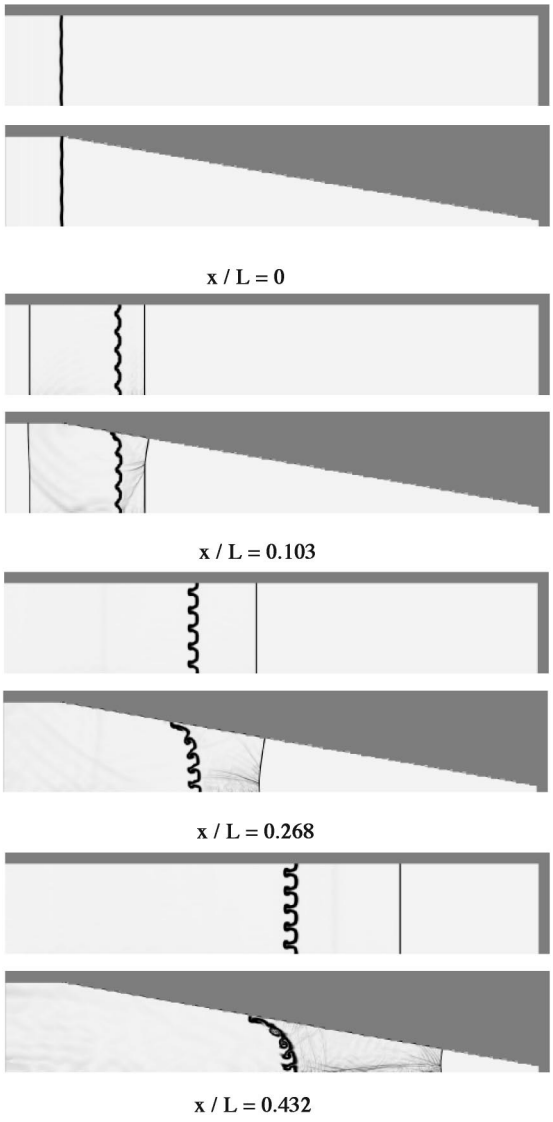

FIG. 23. Numerical simulation: Comparison of the growth of small sinusoidal perturbations in a cylindrical and conical geometry at three locations, x/L. Light–heavy configuration, $M_S=1.56$, L is the cone length extrapolating to the apex.

reflect the role of viscosity in the TMZ growth dynamics. Figure 23 compares the resulting perturbation growth for cylindrical and conical geometries at about the same x/L as the window locations in the experiments. The initial amplitude of the perturbations is 1.25% of the wavelength and there are five wavelengths spanning the radius. The interface geometry in Fig. 23 at various locations indicates that the amplitude growth in both cylindrical and conical geometries is the same. The main difference is the global curving of the interface towards the apex of the cone in the conical geometry. This suggests that the diffuse rear boundary of the interfaces observed in the experiments could be an artifact of this global curving of the interface and hence any enhanced growth could be attributed to it. But, as is evident from the laser-induced scattering results in Fig. 21(b), the interface in the middle of the test section does not have a well-defined rear boundary either.

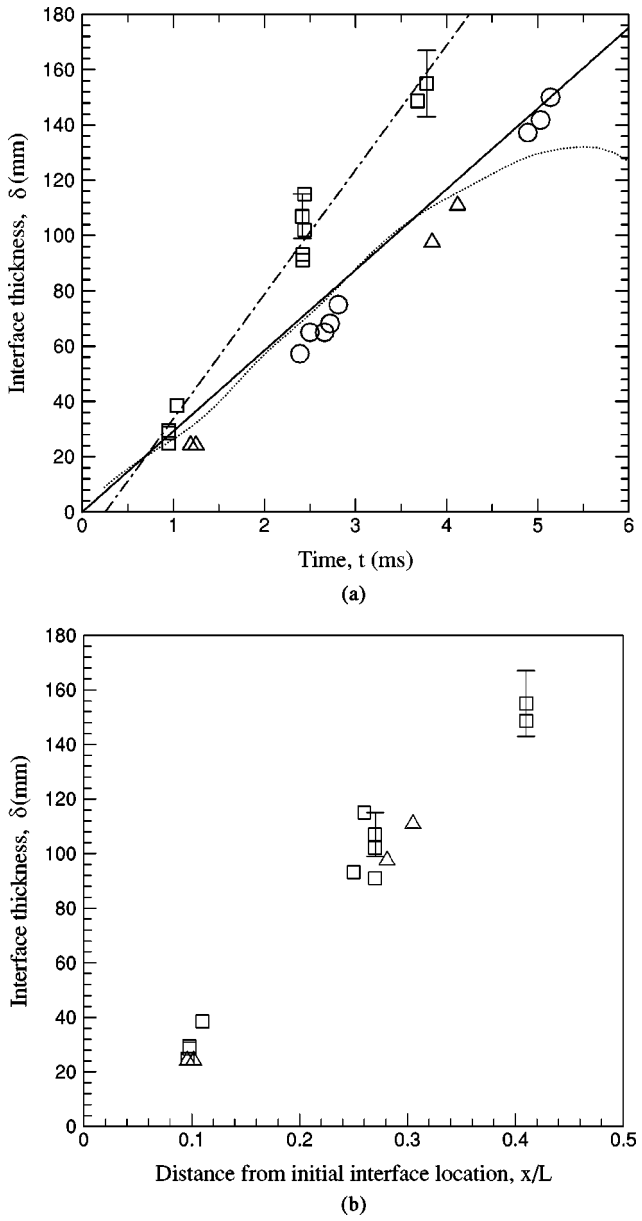

FIG. 24. (a) Growth rate of TMZ in conical geometry along with Vetter's (Ref. 11) data with no convergence; □, $M_S=1.55$; dash-dot line, linear fit; △ $M_S=1.39$; ○, Vetter's data at $M_S=1.50$; purely for reference Mikaelian's Eq. (1) for nonconverging geometry and $M_S=1.55$ is shown as a solid line; dotted line, geometric thickness (obtained as in Fig. 10) for $M_S=1.56$. (b) Interface growth plotted with distance, x/L, $L=1233.5$ mm is the cone length extrapolating to the apex; □, $M_S=1.55$; △, $M_S=1.39$.

D. Growth rate results

The growth of the TMZ thus obtained by the spark schlieren technique is plotted in Fig. 24. Figure 24(a) shows the TMZ growth in time. It is clear that the growth is significantly larger than in Vetter's data at late times. Vetter's[11] data correspond to the same conditions but with no area convergence. His experiment was at a Mach number of 1.5. The data plotted are ''visual thickness'' observed from schlieren photographs. The data from Vetter's graph correspond to his m-(v-h) configuration which means in the initial interface formation the membrane (m) was followed downstream by vertical (v) and horizontal (h) wires. This is also the configuration used in the present experiments. This configuration results in maximum growth rate as compared to his other initial configurations of membrane (m), horizontal wires (h) and vertical wires (v), i.e., v-m-h and (v-h)-m configurations. The reason for this difference was pointed out by Vetter as being possibly due to the smaller damping effect produced by relatively smaller membrane fragments. The interface thickness in the second window location is about 40%–50% larger than in Vetter's data at the same time. Again, this result is based on the TMZ thickness obtained from the pictures and it is possible that some of it is an artifact of global curving of the interface.

A linear fit to $M_S=1.55$ data shown in Fig. 24(a) gives a mean growth rate of 45 m/s which is about 5 m/s larger than that obtained by Vetter[11] after the reflected shock. Also plotted in Fig. 24(a) is Mikaelian's Eq. (1) which is supposed to be valid for late time RM instability growth with no area convergence. The interface velocity used in this equation is 144 m/s obtained from the $x-t$ diagram in Fig. 16 and the post shock Atwood number used is 0.74 obtained from the conditions just after the interaction with the incident shock. Figure 24(a) also shows the evolution of ''geometric thickness'' in the light–heavy configuration at Mach number of 1.56. The ''geometric thickness'' tends to decrease at later times due to the rapid RT stabilizing effect at those times. The plotted ''visual thickness'' in the figure is greater than the ''geometric thickness'' at later times. The diffuse rear end of the interfaces in schlieren images may thus reflect the real nature of the interface in the cone center or it could also be an artifact of the curved interface interacting with the wall boundary layer. However, the shock tube and conditions in the present experiments are the same as those used by Vetter[11] who did not see any boundary layer effects thanks to the large test section size. Figure 24(b) shows the TMZ growth plotted against x/L, L being the length of the cone assumed to be ending at a point. Figure 25 shows the interface thickness with distance in mm along with Vetter's data[11] before the interaction with reflected shock.

IV. SOME COMPUTATIONAL STUDIES

The computations were carried out on the software system AMRITA designed by Quirk.[28] It is a system that automates and packages computational tasks in such a way that the packages can be combined (dynamically linked) according to instructions written in a high level scripting language. The present application uses features of AMRITA that include the automatic construction of different Euler solvers, automatic documentation of the codes, automatic adaptive mesh refinement according to simply chosen criteria, archiving and post-processing of the results. The automation of the assembly and sequencing of the tasks dramatically reduces the possibility of hidden errors. More importantly, it makes computational investigations transparent and testable by others. The ability to change one package at a time, without changing the rest of the scheme, permits easy detection of sources of errors. The scope of the software package far exceeds its use here.

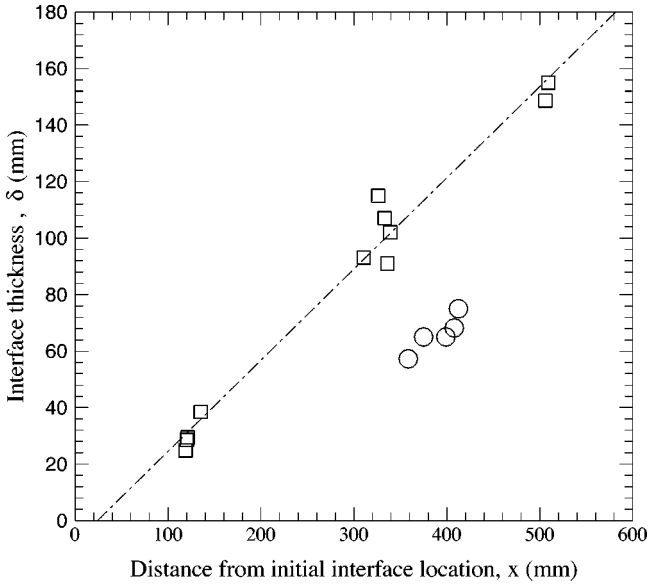

FIG. 25. TMZ growth versus distance from the initial location in mm. Vetter's (Ref. 1) data before interaction with reflected shock are also shown. Dash–dot line is the linear fit; □, $M_S=1.55$; ○, Vetter's (Ref. 11) data at $M_S=1.55$.

Numerical computations using AMRITA were performed on two configurations in a cone with half-angle of 10° to study the interface geometry changes which it experiences as it is convected into the cone. Both light–heavy (LH) and heavy–light (HL) configurations corresponding to air/SF_6 or air/He gas combinations respectively were computed at the same Mach number as in the experiments. The interaction of a plane shock (PS) with a plane interface (PI) is studied. It should be noted that these calculations are Euler calculations and hence do not account for the viscous effects in TMZ growth. The two cases studied computationally are tabulated in Table II.

Figure 26 shows the geometry and location of the interface at various times in case 1. Time $t=0$ always corresponds to the instant when the incident shock reaches the interface. The curving of the interface towards the cone is due to the vorticity deposited on the interface by its interaction with the reflected shock from the triple point. In the last snapshot the interface has almost stopped.

Numerical simulations were also performed in heavy–light configuration (air–He). The simulations were made at Mach number of 1.60 (same as in the experiments). Figure 27 shows snapshots of plane shock and plane interface interaction in heavy–light configuration (case 2). In heavy–light configuration the density gradient is reversed from the light–heavy configurations resulting in the reversal of baroclinic torque arising from the interaction of the interface with the reflected shock, so that the vorticity deposited on the interface is of opposite sign to that of case 1. The interface therefore curves away from the cone, in contrast to case 1. Also, in this case the main wave reflected back into the shock tube at $t=0$ is an expansion wave as expected. The interface comes to a stop much earlier, in this case at $x/L=0.289$ as compared to $x/L=0.575$ in case 1 with light–heavy configuration. The laser-induced scattering image from the experiments in Fig. 21(b) is at about $x/L=0.274$ which is close to the last snapshot of numerical results in Fig. 27.

TABLE II. Two cases studied computationally.

Case no.	Mach no. ±0.01	LH or HL configuration	Shock–interface configuration
1	1.56	LH	PS/PI
2	1.60	HL	PS/PI

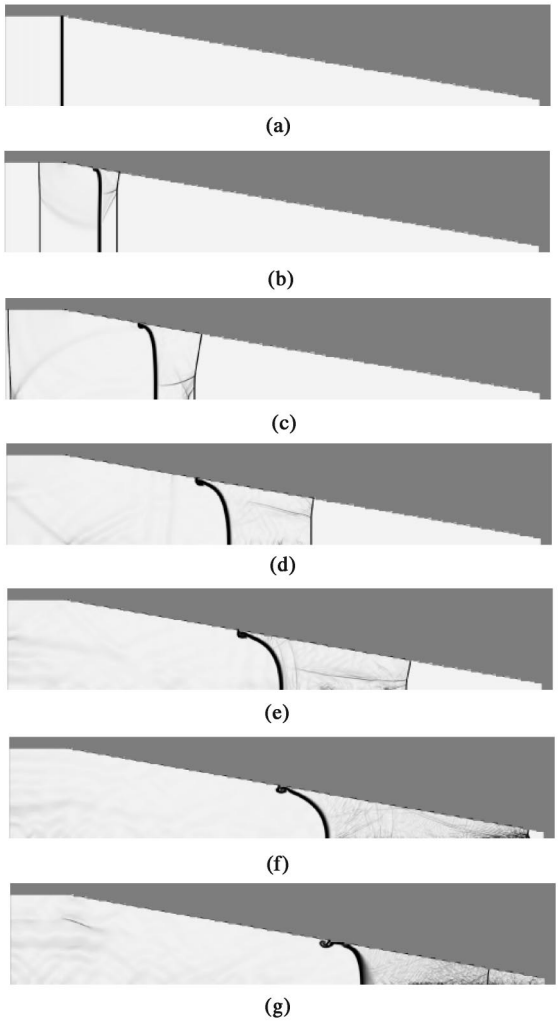

FIG. 26. Numerical simulation: $M_S=1.56$, light–heavy (air–SF_6), plane shock and plane interface. (a) $t=0$, (b) $t=28.505$, (c) $t=71.275$, (d) $t=124.025$, (e) $t=161.403$, (f) $t=204.572$, (g) $t=270.397$ (case 1).

V. CONCLUSIONS

The late-time growth of multimode initial perturbations of a density interface by the Richtmyer–Meshkov instability was studied in a conical geometry. The incident shock forms a Mach reflection at the cone entrance and the reflected shock from the triple point interacts with the interface as it is convected into the cone. The most important and obvious property of the TMZ, its thickness, is measured from schlieren images at three axial locations in light–heavy configurations (air–SF_6) at Mach number of 1.55. Some experi-

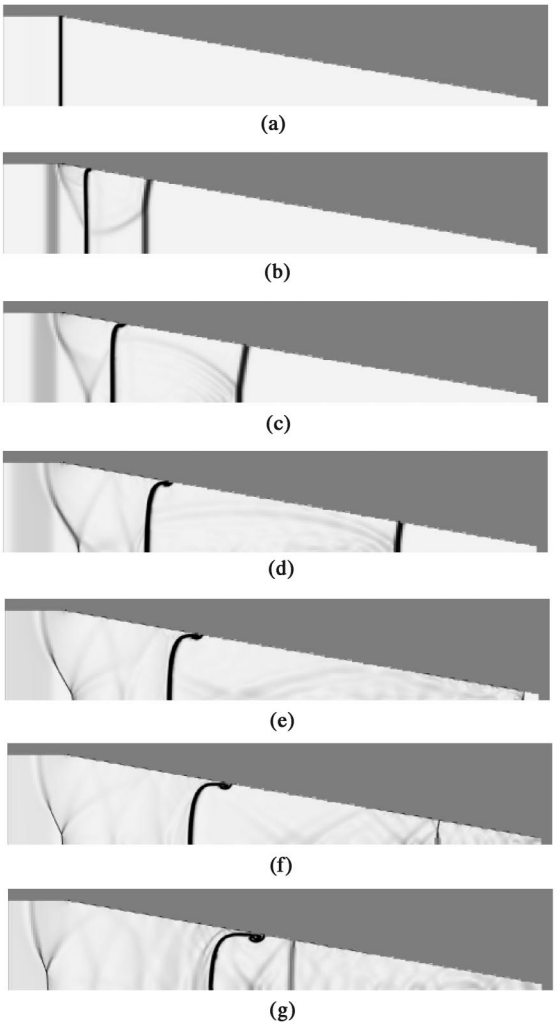

FIG. 27. Numerical simulation: $M_S=1.6$, heavy–light (air–helium), plane shock and plane interface. (a) $t=0$, (b) $t=8.173$, (c) $t=17.105$, (d) $t=30.116$, (e) $t=38.16$, (f) $t=46.191$, (g) $t=57.363$ (case 2).

ments are also done at Mach number of 1.39. The interface first moves into the cone at constant speed, then rapidly decelerates and finally comes to rest due to continuity requirements. Measurements are restricted to the time before the reflection of the main shock from the cone end reaches the interface and before the rapid deceleration starts. A few laser-induced scattering experiments using olive oil fog seeding were also conducted. The conclusions drawn from this study are the following.

(i) Comparison with Vetter's[11] experiments with no area convergence at about the same Mach number showed that the interface thickness was about 40% to 50% larger in the conical geometry. This result is based on the TMZ measurements from schlieren images. The increase in TMZ thickness is attributed to the constant reenergizing of turbulence by the interaction of reflected waves with the interface.

(ii) The dominant scale (blob–eddy size) in the TMZ (as visible in the schlieren images) was 4 mm, which is half the spacing of the wires that support the polymeric membrane. The size of these dominant eddies did not vary with their locations in the TMZ.

(iii) Laser-induced scattering images obtained in the heavy–light configuration showed that the rear of the TMZ is diffuse. This was also found in the schlieren images. The fragments of the polymeric membrane tend to cluster at the front of the interface. This was also the case in the laser-induced scattering image and the schlieren image of experiments with an air–air (Atwood ratio$=0$) interface.

(iv) Inviscid numerical simulations showed that, near the walls, the interface curves toward the apex of the conical test section or away from it, in the light–heavy or heavy–light case, respectively. Numerical simulations of initially perturbed interfaces in cylindrical and conical geometry showed that the vorticity induced growth is the same in the two cases.

ACKNOWLEDGMENTS

The authors would like to thank Professor Joe Shepherd and Professor Mory Gharib of GALCIT for useful discussions during the course of this study. This work was supported by Caltech.

[1] R. D. Richtmyer, "Taylor instability in shock acceleration of compressible fluids," Commun. Pure Appl. Math. **8**, 297 (1960).
[2] E. E. Meshkov, "Instability of the interface of two gases accelerated by a shock wave," Sov. Fluid Dyn. **4**, 101 (1969).
[3] J. D. Lindl and W. C. Mead, "Two dimensional simulation of fluid instability in laser fusion pellets," Phys. Rev. Lett. **34**, 1273 (1975).
[4] Yu. F. Afanas'ev, N. G. Bosov, E. G. Gamalii, O. N. Krokhin, and V. B. Rozanov, "Two dimensional simulation of fluid instability in laser fusion pellets," JETP Lett. **23**, 566 (1976).
[5] J. D. Lindl, R. L. Mc Corry, and E. M. Campbell, "Progress towards inertial confinement fusion," Phys. Today **45** (9), 32 (1992).
[6] J. D. Lindl, *Inertial Confinement Fusion* (AIP, Springer-Verlag, New York, 1998).
[7] L. Smarr, J. R. Wilson, R. T. Barton, and R. L. Bowers, "Rayleigh–Taylor overturn in supernova core collapse," Astrophys. J. **246**, 515 (1975).
[8] G. H. Markstein, "Flow disturbances induced near a slightly wavy contact surface, or flame front, traversed by a shock wave," J. Aerosp. Sci. **24**, 238 (1957).
[9] F. E. Marble, G. J. Hendricks, and E. E. Zukoski, "Progress towards shock enhancement of supersonic combustion process," AIAA Pap. 87-1880 (1987).
[10] I. A. Waitz, F. E. Marble, and E. E. Zukoski, "An investigation of a contoured wall injector for hypervelocity mixing augmentation," AIAA Pap. 91-2265 (1991).
[11] M. Vetter and B. Sturtevant, "Experiments on the Richtmyer–Meshkov instability of an air/SF_6 interface," Shock Waves **4**, 247 (1995).
[12] J. K. Prasad, A. Rasheed, S. Kumar, and B. Sturtevant, "The late time development of Richtmyer–Meshkov instability," Phys. Fluids **12**, 2108 (2000).
[13] K. O. Mikaelian, "Turbulent mixing generated by Rayleigh–Taylor and Richtmyer–Meshkov instabilities," Physica D **36**, 343 (1989).
[14] K. I. Read, "Experimental investigation of turbulent mixing in Rayleigh–Taylor instability," Physica D **12**, 45 (1984).
[15] U. Alon, J. Hecht, D. Ofer, and D. Shvarts, "Power laws and similarity of Rayleigh–Taylor and Richtmyer–Meshkov mixing fronts at all density ratios," Phys. Rev. Lett. **74**, 534 (1995).
[16] G. Dimonte, "Spanwise homogeneous buoyancy-drag model for Rayleigh–Taylor mixing and experimental evaluation," Phys. Plasmas **7**, 2255 (2000).
[17] M. B. Schneider, G. Dimonte, and B. Remington, "Large and small scale structure in Rayleigh–Taylor mixing," Phys. Rev. Lett. **80**, 3507 (1998).
[18] M. Brouillette, "The Richtmyer–Meshkov instability," Annu. Rev. Fluid Mech. **34**, 445 (2002).

[19]H. J. Kull, ''Theory of the Rayleigh–Taylor instability,'' Phys. Rep. **206**, 197 (1991).
[20]H. W. Liepmann, A. Roshko, D. Coles, and B. Sturtevant, ''A 17 in. diameter shock tube for studies in rarefied gas dynamics,'' Rev. Sci. Instrum. **33**, 625 (1962).
[21]M. Brouillette and B. Sturtevant, ''Experiments on Richtmyer–Meshkov instability: Small scale perturbations on a plane interface,'' Phys. Fluids A **5**, 916 (1993).
[22]V. A. Andronov, S. M. Bakhrakh, E. E. Meshkov, V. N. Mokhov, V. V. Nikiforov, A. V. Pevnitskii, and A. I. Tolshmyakov, ''Turbulent mixing at contact surfaces accelerated by shock wave,'' Sov. Phys. JETP **44**, 424 (1976).
[23]R. F. Benjamin, ''Experimental observation of shock stability and shock induced turbulence,'' in *Advances in Compressible Turbulent Mixing, Proceedings of the First International Workshop on the Physics of Compressible Turbulent Mixing*, edited by W. P. Dannevik, A. C. Buckingham, and C. E. Leith (Lawrence Livermore National Laboratory, Livermore, CA, 1992), Conf-8810234, pp. 341-348.
[24]L. Erez, O. Sadot, D. Oron, G. Erez, L. A. Levin, D. Shvarts, and G. Ben-Dor, ''Study of membrane effect on turbulent mixing measurements in shock tubes,'' Shock Waves **10**, 241 (2000).
[25]S. Kumar, ''An experimental investigation of Richtmyer–Meshkov instability,'' Ph.D. thesis, California Institute of Technology, 2003.
[26]R. E. Setchell, E. Storm, and B. Sturtevant, ''An investigation of shock strengthening in a conical convergent channel,'' J. Fluid Mech. **56**, 505 (1972).
[27]S. I. Abarzhi, ''Nonlinear evolution of unstable fluid interface,'' Phys. Rev. E **66**, 036301 (2002).
[28]J. J. Quirk, ''Amrita—a computational facility (for cfd modelling),'' in VKI 29th. CFD Lecture Series (Von Karman Institute for Fluid Dynamics, 1998).
[29]M. Brouillette and B. Sturtevant, ''Growth induced by multiple shock waves normally incident on plane gaseous interfaces,'' Physica D **37**, 248 (1989).
[30]M. Brouillette, ''On the interaction of shock waves with contact surfaces between gases of different densities,'' Ph.D. thesis, California Institute of Technology, 1989.
[31]M. Brouillette and B. Sturtevant, ''Experiments on Richtmyer–Meshkov instability: Small scale perturbations on a continuous interface,'' J. Fluid Mech. **263**, 271 (1994).
[32]O. Sadot, L. Erez, D. Alon, L. Oron, L. A. Levin, G. Erez, G. Ben-Dor, and D. Shvarts, ''Study of nonlinear evolution of single-mode and two bubble interaction under Richtmyer–Meshkov instability,'' Phys. Rev. Lett. **80**, 1654 (1998).